Shape memory alloys cyclic behavior : experimental study and modeling

Pierrick Malecot, Christian Lexcellent, Emmanuel Foltete, Manuel Collet

Shape Memory Alloys Cyclic Behavior: Experimental Study and Modeling

P. Malécot[1], C. Lexcellent, E. Foltête, M. Collet

Laboratoire de Mécanique Appliquée, FEMTO-ST Université de Franche-Comté, Besancon, France

Shape memory alloys (SMA) are good candidates for being integrated in composite laminates where they can be used as passive dampers, strain sensors, stiffness or shape drivers. In order to improve the SMA modeling and develop the use of these alloys in structural vibration control, better understandings of cyclic behavior and thermal dissipation are needed. The present study investigates experimentally the cyclic behavior of SMA and more particularly, the influence of strain rates on three different materials. The thermal dissipation aspect is also studied using an infrared camera. A phenomenological model based on the RL model (Raniecki, B., Lexcellent, C., 1994, "RL Models of Pseudoelasticity and Their Specification for Shape Memory Solids." Eur. J. A/Solids, 13, pp. 21–50) is then presented with the intention of modeling the behavior's alterations due to the cycling. By introducing the thermodynamic first principle, a study of the heat equation is developed in order to predict the temperature evolution during a cyclic tensile test. Furthermore, in order to model the damping effect created by the hysteresis phenomenon and the stiffness variation due to the phase transformation, an equivalent nonlinear complex Young's modulus is introduced. This notion usually used for viscoelastic materials is adapted here to SMA. Moreover, the impact of cycling on the equivalent modulus is presented. As a conclusion, a numerical results panel obtained with the phenomenological cyclic SMA model, the heat equation, and the equivalent complex Young modulus is presented.

Keywords: shape memory alloys, cyclic behavior, thermal dissipation, thermomechanical modeling, nonlinear modeling

1 Introduction

The phase transformation from a mother phase called austenite to a product phase called martensite in the shape memory alloys (SMA) makes them potential candidates for vibration damping systems. SMA are already studied for applications in structural vibration control [1] and as vibration dampers for example in seismic applications [2,3]. From a mechanical point of view we can distinguish, to explain this potential, two different phenomena linked to the phase transformation: the existence of an hysteresis and a stiffness variation. In order to understand the impact of these two phenomena on the dynamic of a system, a first study was presented in [4]. In this previous work, an equivalent nonlinear complex Young's modulus was used to quantify the balanced harmonic response of the material. It was calculated using a simplified RL model [5] without taking into account the modification of the behavior with the cycling and the strain rate. A new phenomenological model is developed in the present paper in order to take into account the SMA behavior alteration due to the cycling. Basically, an experimental study is performed in order to quantify the SMA behavior modification generated by the cycling and the strain rate. This experimental study allows to analyze the thermal dissipation and the evolution of the hysteresis width. A review of the literature about experimental works on SMA cyclic behavior [6–9] led to the conclusion that no previous experimental study had been driven on Cu–Al–Be SMA, so we mainly used this material to enlarge our skills field.

The present paper is divided into 4 parts:

1. A complete experimental study is presented. First, a Ni–Ti alloy was briefly studied by performing a quasistatic cyclic tensile test and a tensile cyclic test at 5 Hz with increasing maximum strain. These tests were mainly performed on JRC-ISPC in ISPRA (Italy). Then two Cu–Al–Be were studied, the first one was austenitic at room temperature and the second one was martensitic at room temperature. For these two materials, large strain rate amplitudes were applied on cyclic tensile tests. Moreover an infrared camera was used to measure the temperature variation on the sample surface during each test.
2. A phenomenological cyclic thermomechanical model is developed. This modeling is based on the general thermodynamic framework built by Raniecki and Lexcellent [5] where three internal variables have been introduced: the residual stress, the residual strain, and the volume fraction of residual martensite at free stress state accumulated during the cycling. In order to complete this part, a modeling of the thermal dissipation during cyclic tests is developed by performing a study based on the heat equation.
3. In this part the concept of equivalent complex Young's modulus is introduced in order to describe the damping and the stiffness of the SMA samples. Therefore this modulus is linked to the phenomenological model through the strain energy densities over one period and one quarter of a period.
4. The numerical predictions given by the cyclic thermomechanical model are presented and compared to the experimental results. The impact of the phenomenological cyclic modeling on the equivalent complex Young's modulus real and imaginary parts is discussed. Finally, temperature variation predictions are presented.

[1]Corresponding author.

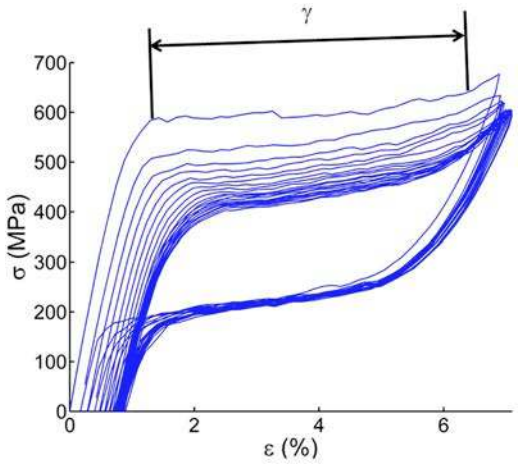

Fig. 1 Ni–Ti cyclic test at 25°C, $\dot{\varepsilon}=10^{-4}\ s^{-1}$

2 Experimental Study of Cyclic Processes

The first for modeling the cyclic behavior of SMA is to build a database with experimental tests on different materials. Three different materials were studied: a Ni–Ti and two Cu–Al–Be. The Ni–Ti and the first Cu–Al–Be were austenitics at room temperature while the second Cu–Al–Be was martensitic at room temperature. These three materials allowed to explore a large field of SMA behaviors in order to quantify the effect of cycling and the strain rate impact.

2.1 Ni–Ti Study. For this material the tests were performed partly in our laboratory on an electrical powered tensile machine Instron 6250. The other part of the tests was done on the JRC-ISPC laboratory tensile machines. Both of these tests were performed on 2 mm diameter Ni–Ti wires.

2.1.1 Quasistatic Cyclic Tests. This test was performed at a strain rate of 10^{-4} s^{-1}. On the strain-stress curve in Fig. 1 we can observe all the "classical" elements of a cyclic test. The first element to notice is the decrease of the outset of the direct phase transformation with the number of cycles. For the outset of the reverse phase transformation, no significant variation occurs during the cycling (Fig. 2). The second important fact to point out is a residual strain remaining for a free stress state. At last after a given number of cycles the sample tends to reach a stabilized behavior.

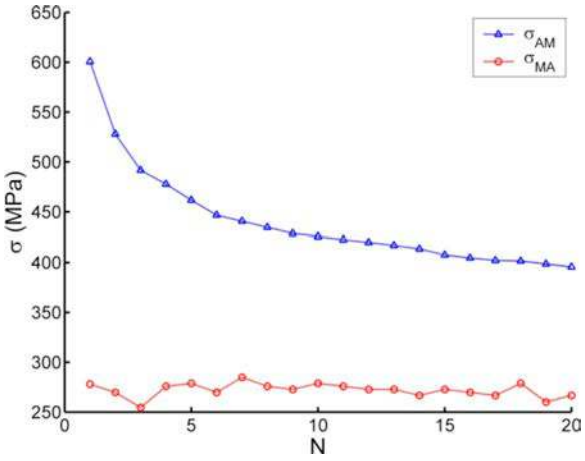

Fig. 2 σ_{AM} and σ_{MA} variation with the number of cycles for Ni–Ti

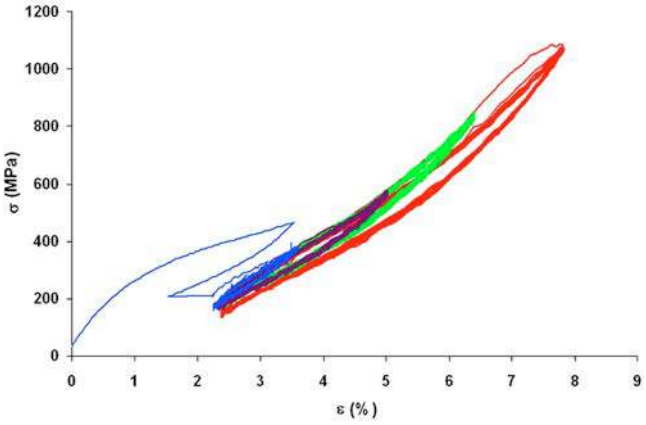

Fig. 3 Ni–Ti dynamic test at 25°C and 5 Hz with $\Delta\varepsilon_1=1.4\%$, $\Delta\varepsilon_2=2.8\%$, $\Delta\varepsilon_3=4.2\%$, $\Delta\varepsilon_4=5.6\%$

Basically for all the observed parameters the most important variation occurred between the first and the second cycle and less significantly between the second and third cycle, then the parameters variations are slower.

2.1.2 Strain Rate Influence. In order to study the strain rate impact and the maximum strain influence, the test presented in Fig. 3 was performed. The sample was loaded under a cyclic, tensile deformation with an increasing maximum strain from 3.5% to 8% at a frequency of 5 Hz (the equivalent strain rates are given in Table 1). The shape of the cycles is very different from the one observed on the quasistatic tests. The phase transformation plateaus for direct and reverse transformations have disappeared. Moreover the area of the cycles is smaller and the stress reached for a strain of 7% is about 900 MPa versus 700 MPa for quasistatic tests.

From a thermal point of view a huge increase of the temperature (Fig. 4) from 25°C to 60°C can be noticed. Furthermore the slope of the temperature curve increases with the increase of the maximum stress. For this test the temperature variation was measured by a thermal probe.

Table 1 Equivalent strain rate for a frequency of 5 Hz

Maximum strain (%)	3.5	5	6.5	8
Equivalent strain rate 10^{-1} s^{-1}	1.2	2.7	4.2	5.7

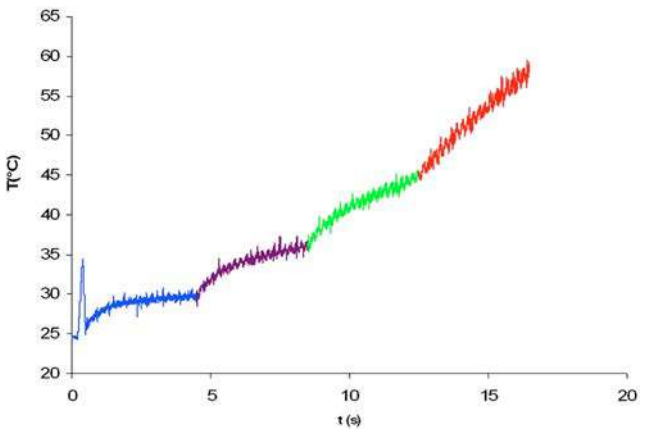

Fig. 4 Ni–Ti dynamic test (5 Hz): temperature variation

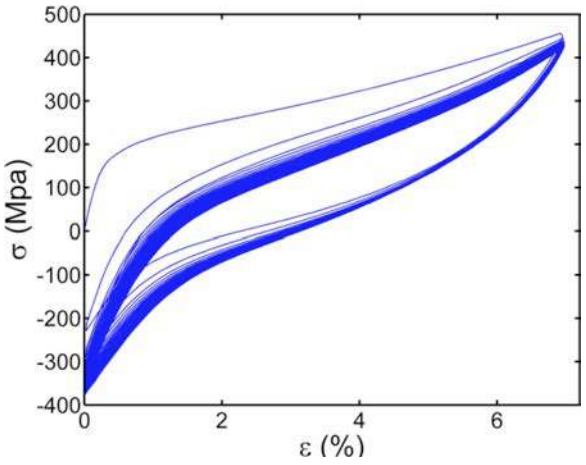

Fig. 5 Cu–Al–Be(1) cyclic test at 22 °C, $\dot{\varepsilon}=10^{-4}$ s^{-1}

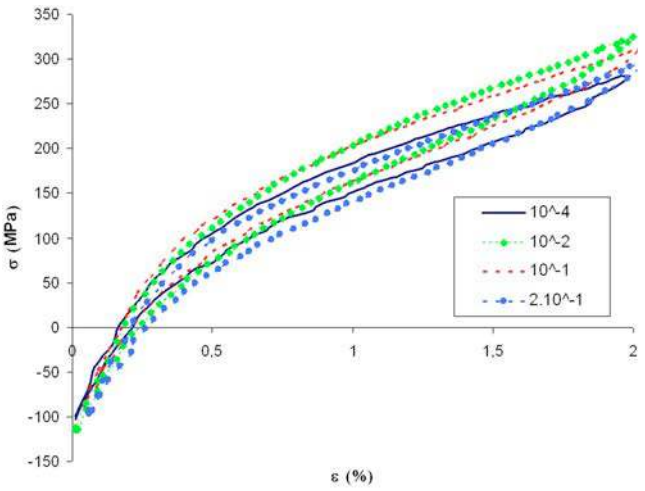

Fig. 6 Cu–Al–Be(1) stabilized cycles comparison after 100 cycles

2.2 Cu–Al–Be Austenitic at Room Temperature. The second tested material is a Cu–Al–Be in austenitic phase at room temperature (Cu–Al–Be(1)). The tests performed on this material were done on an hydraulic powered tensile machine referenced Instron 8501. The maximum strain was imposed and controlled by an extensometer. In order to measure the thermal dissipation a CEDIP infrared system was used. This system consists of an infrared camera referenced Jade MWIR and the ALTAIR software [10]. Cylindrical Cu–Al–Be samples designed for tensile-compression tests were used. The samples were loaded under a cyclic, tensile, sinusoidal deformation between the strains of 0% and 7%. It is important to underline that each test was performed on a virgin sample.

2.2.1 Quasistatic Cyclic Tests. This test was performed at a strain rate of 10^{-4} s^{-1}. On the Cu–Al–Be strain-stress curves (Fig. 5) almost the same behaviors than for Ni–Ti can be observed: decrease of the outset of the direct phase transformation, decrease of the cycle area with the number of cycles, and no significant variation of the outset of the reverse phase transformation. Nevertheless an important difference can be underlined: the residual strain at a free stress state is more important, 3% for the Cu–Al–Be versus 1% for the Ni–Ti. At last it is important to notice the "memory point" aspect, also called "return memory point" by Ortin [11] (i.e., at the end of the loading for each cycle the sample finds back the same stress-strain state; 440 MPa for 7%).

Like for the Ni–Ti the most important variation for all the observed parameters occurred between the first and the second cycle and less significantly between the second and third cycle.

2.2.2 Strain Rate Influence on Mechanical Behavior. In order to study the strain rate influence on the cyclic behavior of this material, cyclic, tensile, sinusoidal tests were performed at four different strain rates (including quasistatic tests) from 10^{-4} s^{-1} to 2×10^{-1} s^{-1}, the results are given in Fig. 6. In this figure the shape of the hysteresis for each strain rate are compared after 100 cycles. For Piedboeuf et al. [9] the mechanical behavior is stabilized after 100 cycles. After the study of the superposition of the four stabilized cycles for this Cu–Al–Be it is clear that the strain rate has no significant influence when it comes to compare of shape, area and apparent slope of the stabilized hysteresis cycle.

2.2.3 Strain Rate Influence on Thermal Dissipation. For the first test at 10^{-4} s^{-1} Fig. 7(*a*) shows an isothermal profile during the cycling, and the temperature variation is around 0.2 °C which is not significant compared to the room temperature variation. For the second test at 10^{-2} s^{-1} the thermal profile is different (Fig. 7(*b*)), the first cycle reaches the maximum temperature of 27.5 °C. Then, the maximum temperature decreases cycle after cycle to reach 26.5 °C in the stabilized state. During each cycle of this test the temperature variation is about 4 °C. The last two tests at 10^{-1} s^{-1} and 2×10^{-1} s^{-1} exhibit the same thermal profile (Figs. 8(*a*) and 8(*b*)) the temperature constantly increases during the cycling even after more than 200 cycles. Compared to the room temperature, the increase is about 4 °C after 50 cycles. The differences between the tests come from the different equilibrium between the heat diffusion produced by the phase transformation in

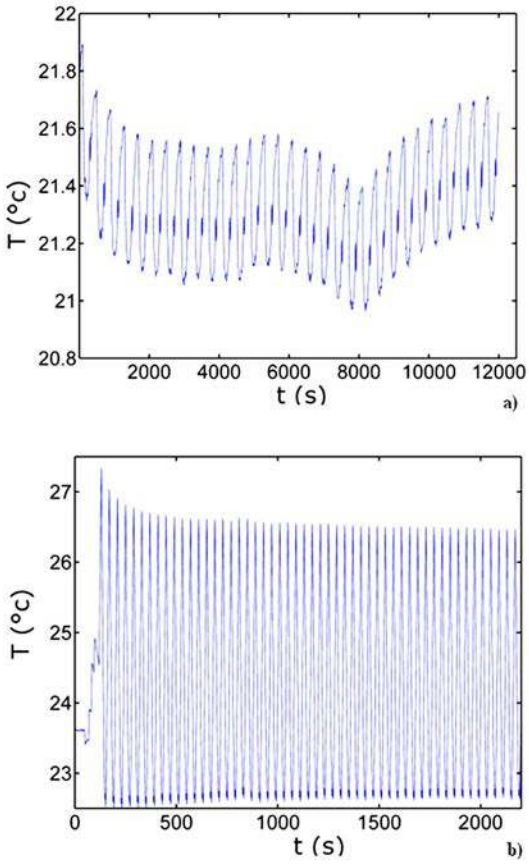

Fig. 7 Cu–Al–Be(1) temperature variation: (*a*) test at 10^{-4} s^{-1}; (*b*) test at 10^{-2} s^{-1}

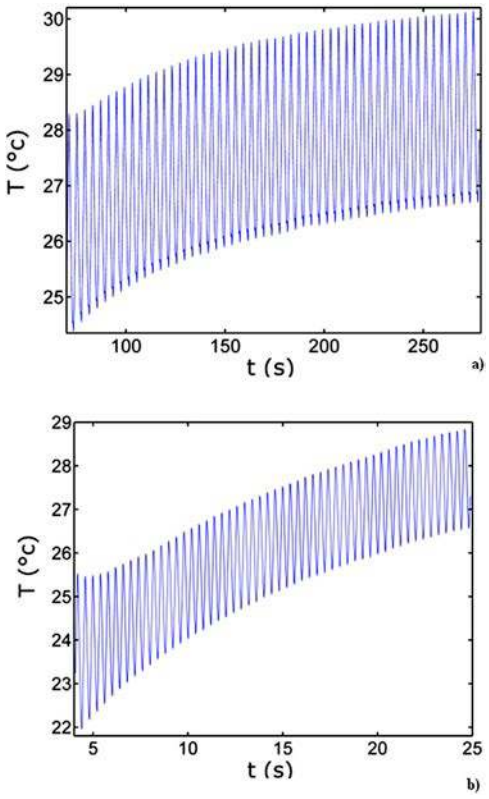

Fig. 8 Cu–Al–Be(1) temperature variation: (*a*) test at 10^{-1} s^{-1}; (*b*) test at 2×10^{-1} s^{-1}

the material and the heat dissipation capacity of the boundaries.

This experimental study demonstrates that for an increasing strain rate the used Cu–Al–Be has a different behavior than the Ni–Ti. For this Cu–Al–Be there is no significant change of the stabilized cycle when the strain rate is multiplied by 2000, whereas the thermal dissipation is greatly influenced.

2.3 Cu–Al–Be Martensitic at Room Temperature. Finally, in order to complete the experimental database, a Cu–Al–Be martensitic at room temperature was tested (Cu–Al–Be (2)). The testing conditions for this material are the same than previously. In a practical way, the samples were prestrained at 1.65% and loaded under a cyclic, tensile, sinusoidal deformation between the strains of 1.30% and 2%. It is important to underline that each test was performed on a virgin sample.

2.3.1 Quasistatic Cyclic Tests. The material behavior is very different from the two others. Indeed this material is martensitic at room temperature and there is no phase transformation during the cycling but martensite reorientation. As shown in Fig. 9, the stress-strain curve given by this quasistatic test at 10^{-4} s^{-1} is very different from the other quasistatic curves (Figs. 1 and 5). A small decrease of the cycle area and a significant variation of the sample stiffness during the cycling can be observed. It is relevant to notice once again that for all the observed parameters the most important variation occurred between the first and the second cycle and less significantly between the second and third cycle. Finally, after a given number of cycles the sample tends to reach a stabilized behavior.

2.3.2 Strain Rate Influence on Mechanical Behavior. For this material the previous method was used in order to study the strain rate impact on the cyclic behavior: cyclic, tensile, sinusoidal tests at four different strain rates (including quasi static tests) from 10^{-4} s^{-1} to 10^{-1} s^{-1} were performed. The results are given in Fig. 10 where the shape of the stabilized cycle obtained after

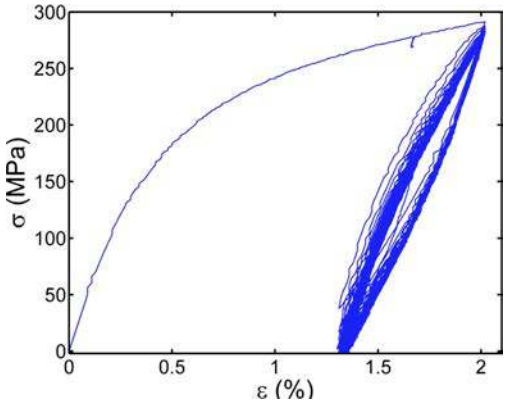

Fig. 9 Cu–Al–Be(2) quasistatic cyclic test at 22°C

100 cycles are compared for each strain rate. The superposition of the four stabilized cycles shows no significant influence when it comes to compare shape, area, and apparent slope.

2.3.3 Strain Rate Influence on Thermal Dissipation. For this material each strain rate gives a different thermal curve. For the quasistatic-test (Fig. 11(*a*)) a temperature variation between 22.25°C and 22.5°C can be observed for each cycle (the room temperature is around 22.3°C). For the second test (Fig. 11(*b*)), at a strain rate 10 times higher, the first cycle reaches the maximum temperature of the test (24.75°C). Then the maximum temperature decreases during around 10 cycles, afterwards it is stabilized between 24.15°C and 24.55°C (the room temperature is around 24.5°C). For the third test (Fig. 12(*a*)) at 10^{-2} s^{-1} the reverse phenomenon can be noticed. Attention can be paid to an increase of the temperature during 20 cycles from the room temperature (25.25°C) to a maximum temperature of 26°C. After these 20 cycles the temperature variation is stabilized between 25.6°C and 26°C. The last test (Fig. 12(*b*)) shows a constant increase of the temperature from 26°C to 30°C, and there is no temperature stabilization after more than 200 cycles.

As a conclusion to this experimental set it is important to highlight that for this Cu–Al–Be the heat produced by the sample does not come from phase transformation but from martensite platelets rubbing and less significantly from martensite platelets reorientation. Besides no significant differences are observed for this ma-

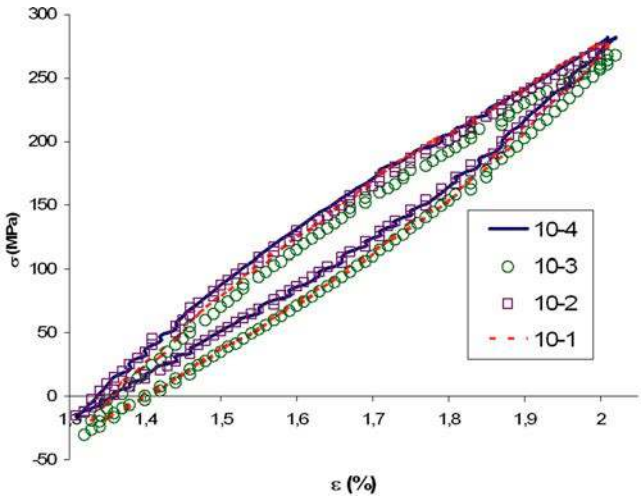

Fig. 10 Cu–Al–Be(2) stabilized cycle's comparison after 100 cycles

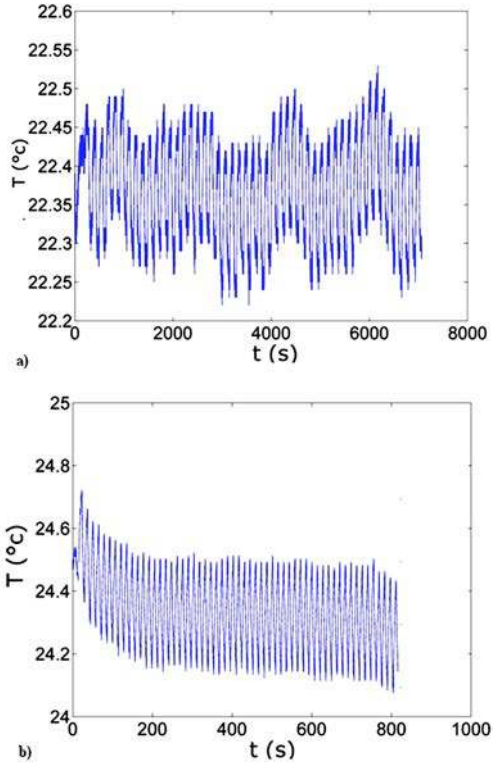

Fig. 11 Cu–Al–Be(2) temperature variation: (*a*) test at 10^{-4} s^{-1}; (*b*) test at 10^{-3} s^{-1}

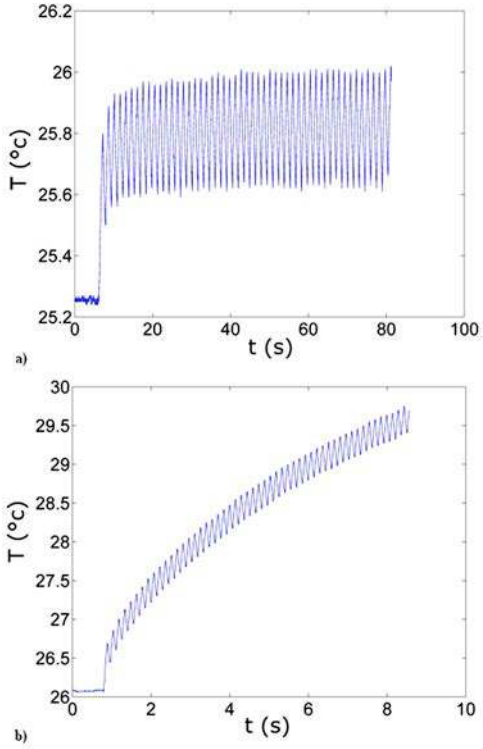

Fig. 12 Cu–Al–Be(2) temperature variation: (*a*) test at 10^{-2} s^{-1}; (*b*) test at 10^{-1} s^{-1}

terial between stabilized cycles when the strain rate is multiplied by 1000, but an important impact of the strain rate on the heat dissipation can be underlined.

2.4 Conclusions. Large amplitudes of strain rates on three different materials have been studied. The three materials show different behaviors. The more sensitive material to the strain rate increase is the Ni–Ti with a huge heat dissipation and a significant decrease of the hysteresis cycle area leading to a decrease of the dissipated mechanical energy. For the two Cu–Al–Be similar conclusions can be done: there is no significant influence of the strain rate on the mechanical behavior but a relevant influence on the thermal dissipation. The martensitic Cu–Al–Be at room temperature proves to be more stable during the cycling, that is why this material seems to have a great potential for structural damping.

3 Modeling of Cyclic Behavior

A few good models exist in the literature [12–15] to model the cyclic behavior of SMA. An improved version of the model proposed by Lexcellent and Bourbon [12] is first developed here. Then as the experimental results presented in this paper show the importance of the thermal diffusion, a complete heat equation study based on the first principle of the thermodynamic (the conservation law) is presented.

3.1 Cyclic Thermomechanical Modeling. This modeling of the SMA cyclic behavior is based on the general thermodynamic framework used by Raniecki and Lexcellent [5] in the R_L model. Furthermore, the present modeling uses parts of the unified SMA model by Leclerq and Lexcellent [16]. The main hypothesis of this unified model is to distinguish two kinds of martensites: the oriented martensite z_σ and the self-accommodating martensite z_T with

$$z = z_\sigma + z_T \tag{1}$$

3.1.1 Residual Martensite. A new hypothesis is added to the R_L model: the residual strain at a free stress state after a given number of loading and unloading is given by the volume fraction of residual martensite. In order to link this two parameters the same kind of relation than the usual behavior law $\varepsilon_{tr} = \gamma \cdot z_\sigma$ can be used, where γ is the maximum strain associated to a complete phase transformation during a tensile test,

$$\varepsilon_{ir} = \gamma \,.\, h \tag{2}$$

where ε_{ir} is the residual strain at $\sigma = 0$, h is the fraction of residual martensite. The difference between h and z is similar to the difference between the notions of total and permanent strains in the classical theory of plasticity. The introduction of this new variable involves a few hypotheses about its variation. We assume that the existence and growing of *the* residual fraction of martensite are dependent on the volume fraction of oriented martensite,

$$\dot{z}_\sigma > 0 \qquad \dot{h} \geqslant 0$$

$$\dot{z}_\sigma \leqslant 0 \qquad \dot{h} = 0 \tag{3}$$

We also stipulate a second hypothesis concerning the existence of a stabilized cycle; this hypothesis is confirmed by the experiments presented in the previous part of this paper and by the work of Myazaki [17]. This hypothesis imposes a saturation value h_∞ for the residual martensite.

3.1.2 Modeling. The model is developed by writing the specific free energy of the system at a nonequilibrium state. The system consists of three phases: (1) the mother phase austenite, (2) the self-accommodating martensite, (3) the oriented martensite. The specific free energy of each phase is defined by

$$\phi^{(1)} = u_0^{*(1)} - T\,.\,s_0^{*(1)} + \frac{E}{2\,.\,\rho}(\varepsilon^{(1)} - \varepsilon_T^{(1)})^2 + C_v\left(T - T_0 - T\cdot\ln\left(\frac{T}{T_0}\right)\right) + \phi_h^{*(1)}$$

$$\phi^{(2)} = u_0^{*(2)} - T\,.\,s_0^{*(2)} + \frac{E}{2\,.\,\rho}(\varepsilon^{(2)} - \gamma\,.\,z - \varepsilon_T^{(2)})^2 + C_v\left(T - T_0 - T\cdot\ln\left(\frac{T}{T_0}\right)\right) + \phi_h^{*(2)}$$

$$\phi^{(3)} = u_0^{*(3)} - T\,.\,s_0^{*(3)} + \frac{E}{2\,.\,\rho}(\varepsilon^{(3)} - \gamma\,.\,z - \varepsilon_T^{(3)})^2 + C_v\left(T - T_0 - T\cdot\ln\left(\frac{T}{T_0}\right)\right) + \phi_h^{*(3)} \tag{4}$$

The term $\phi_h^{*(\alpha)}$ is the contribution of the cycling to the free energy, and is defined by the equation

$$\phi_h^{*(\alpha)}(h,T) = u_h^{*(\alpha)} - T\,.\,s_h^{*(\alpha)} \quad \text{avec } \phi_h^{*(\alpha)}(0,T) = 0 \tag{5}$$

The specific free energy of the system is written as follows:

$$\phi = (1-z)\phi^{(1)} + z_T\phi^{(2)} + z_\sigma\phi^{(3)} + \Delta\phi \tag{6}$$

with

$$\Delta\phi = z_T(1-z)\phi^{12} + z_\sigma(1-z)\phi^{13} + z_T z_\sigma\phi^{23} \tag{7}$$

where $\phi^{\alpha\beta}$ is the energy of interaction between phases α and β. It is important to underline that the two kinds of martensite cannot be distinguished from a physical point of view so

$$\phi^{12} = \phi^{13} = \phi^{it}$$

$$\phi^{23} = \phi_m^{it}$$

$$u_0^2 = u_0^3 = u_0^m$$

$$s_0^2 = s_0^3 = s_0^m \tag{8}$$

Thus, at a constrained equilibrium state, the specific free energy of the system can be written:

$$\phi(\varepsilon,T,z_T,z_\sigma,h) = \frac{E}{2\,.\,\rho}(\varepsilon - \gamma\,.\,z_\sigma - \varepsilon_T)^2 + C_v\left((T-T_0) - T\ln\left(\frac{T}{T_0}\right)\right) + \phi^*(T,z) + \phi_{tr}(T,z,h) \tag{9}$$

with

$$\phi^*(T,z) = u_0^{*(1)} - T\,.\,s_0^{*(1)} - z\Pi_0^f(T) + \Delta\phi$$

$$\phi_{tr}(h,T,z) = \phi_h^{*(1)} - z\Delta\Pi_0^f(h,T) \tag{10}$$

where $\phi_{tr}(h,T,z)$ is the free energy decrease generated by the cycling, and with

$$\Delta\Pi_0^f(h,T) = \Delta u_h^*(h) - T\Delta s_h^*(h)$$

$$\Delta u_h^{*(1)}(h) = u_h^{*(1)}(h) - u_h^{*(3)}(h)$$

$$\Delta s_h^{*(1)}(h) = s_h^{*(1)}(h) - s_h^{*(3)}(h)$$

$$\Pi_0^f(T) = (u_0^{*(1)} - u_0^{*(2)}) - T(s_0^{*(1)} - s_0^{*(2)}) \tag{11}$$

For this system the Clausius-Duhem inequality is the following:

$$\left(\sigma - \rho\,.\,\frac{\partial\phi}{\partial\varepsilon}\right)\dot{\varepsilon} - \rho\,.\left(s + \frac{\partial\phi}{\partial T}\right)\dot{T} - \rho\frac{\partial\phi}{\partial z_\sigma}\dot{z_\sigma} - \rho\frac{\partial\phi}{\partial z_T}\dot{z_T} - \rho\,.\,\frac{\partial\phi}{\partial h}\dot{h} \geqslant 0 \tag{12}$$

So, the entropy and the stress are written

$$s = -\frac{\partial\phi}{\partial T} = \frac{\alpha_0\sigma}{\rho} + C_v\ln\left(\frac{T}{T_0}\right) + z(1-z)\overline{s_0} + s_0^{*(1)} - z\Delta s^* + s_h^{*(1)}(h) - z\Delta s_h(h) \tag{13a}$$

$$\sigma = \rho\,.\,\frac{\partial\phi}{\partial\varepsilon} = E(\varepsilon - \gamma z - \alpha_0(T-T_0)) \tag{13b}$$

The three thermodynamical forces associated to z_σ, z_T, and h are

$$\Pi_\sigma^f = -\frac{\partial\phi}{\partial z_\sigma} = \Pi_0^f + \frac{\gamma\,.\,\sigma}{\rho} - (1-2z)\phi_{it} - z_T\phi_{it}^m + \Delta\Pi_0^f(h,T)$$

$$\Pi_T^f = -\frac{\partial\phi}{\partial z_T} = \Pi_0^f + \frac{\gamma\,.\,\sigma}{\rho} - (1-2z)\phi_{it} - z_\sigma\phi_{it}^m$$

$$\Pi^h = -\frac{\partial\phi}{\partial h} = -\frac{\partial\phi_{tr}}{\partial h} = z\frac{\partial(\Delta\Pi_0^f(h\,.\,T))}{\partial h} - \frac{\partial\phi_h^{*(1)}}{\partial h} \tag{14}$$

Moreover, by introducing

$$\begin{cases} u_h^{*(2)}(h) = \frac{1}{2}\bar{\bar{u}}_2h^2 - \overline{u_2}h \\ s_h^{*(2)}(h) = \frac{1}{2}\bar{\bar{s}}_2h^2 - \overline{s_2}h \end{cases} \tag{15}$$

$$\begin{cases} \bar{\bar{\phi}}(T) = \bar{\bar{u}}_2 - T\,.\,\bar{\bar{s}}_2 \\ \bar{\phi}(T) = \overline{u}_2 - T\overline{s}_2 \end{cases} \tag{16}$$

we obtain

$$\Delta\Pi_0^f = -\frac{1}{2}\bar{\bar{\phi}}h^2 + \bar{\phi}h \tag{17}$$

The existence of a stabilized cycle implies

$$\text{when } h \to h_\infty \quad \frac{\partial\Delta\Pi_0^f}{\partial h} = 0 \qquad h_\infty = \frac{\bar{\phi}}{\bar{\bar{\phi}}} \tag{18}$$

The complete description of the evolution of the thermodynamical behavior requires the knowledge of the kinetics equations for the two variables z and h. They should be formulated in a way such that the Clausius Duhem inequality is satisfied

$$dD = \Pi_\sigma^f dz_\sigma + \Pi_T^f dz_T + \Pi^h dh \geqslant 0 \tag{19}$$

where dD is the infinitesimal energy dissipation.

3.1.3 Transformations Kinetics. By analogy with classical plasticity, four yield functions are defined: Ψ_{AM}^α for the direct transformation and Ψ_{MA}^α for the reverse one, with $\alpha=\sigma$ for the oriented martensite and $\alpha=T$ for the self-accommodated martensite. These functions are defined by

$$\psi_{AM}^\sigma = \Pi_\sigma^f - k_{AM}^\sigma$$

$$\psi_{MA}^\sigma = -\Pi_\sigma^f + k_{MA}^\sigma$$

$$\psi_{AM}^T = \Pi_T^f - k_{AM}^T$$

$$\psi_{MA}^\sigma = -\Pi_T^f + k_{MA}^T \tag{20}$$

Reporting to the model developed by Leclerq [16], and applied to a cyclic loading, the functions k are defined by

$$k_{AM}^\sigma = 2\phi_{it}\frac{z_\sigma - z_\sigma^m - h}{1-h} - \frac{\Delta s^*}{a_{AM}^\sigma}\log\frac{1-z_\sigma+z_\sigma^m}{1-h} - \Delta s^*\left[(T-T^*) + \frac{b_{AM}}{b_m^*}(\exp(-b_m^*(T-M_s^0)) - \exp(-b_m^*(T^*-M_s^0)))\right] \tag{21a}$$

$$k_{MA}^{\sigma} = 2\phi_{it}\frac{1-z_\sigma+z_\sigma^m}{1-h} - \frac{\Delta s^*}{a_{MA}^{\sigma}}\log\frac{z_\sigma - z_\sigma^m - h}{1-h} - \Delta s^*\Bigg[(T-T^*) + \frac{b_{MA}}{b_m}(\exp(-b_m(T-A_s^0)) - \exp(-b_m(T^*-M_s^0)))\Bigg] \quad (21b)$$

and

$$k_{AM}^{T} = 2\phi_{it}(z_T - z_T^m) - \frac{\Delta s^*}{a_{AM}^{T}}\log(1-z_T+z_T^m) \quad (22a)$$

$$k_{MA}^{T} = 2\phi_{it}(z_T - z_T^m - 1) - \frac{\Delta s^*}{a_{MA}^{T}}\log(z_T - z_T^m) \quad (22b)$$

with a_β^α, b_β, b_m^*, b_m ($\alpha=\sigma$, T and $\beta=AM$, MA) material parameters, and T^* is the initial temperature.

The h parameter kinetic must satisfy three properties: 1. h_∞ must exist; 2. $dh \geqslant 0$ when $dz_\sigma > 0$; 3. $dh=0$ when $dz_\sigma \leqslant 0$.

The simplest kinetic to comply with these properties is

$$dh = m_0(h_\infty - h)^p \,.\, \langle dz_\sigma \rangle \quad \text{where} \begin{cases} \langle x \rangle = x & if\ x \geqslant 0 \\ \langle x \rangle = 0 & if\ x < 0 \end{cases} \quad (23)$$

The identification of all the necessary parameters is fully explained in [12,16]. Equation (20) permits us to define the transformation phases yield function and direction, so with Eqs. (21)–(23) we are now able to completely model the cyclic behavior of a shape memory alloy.

3.2 Thermal Dissipation Modeling. This part presents a complete study of the heat equation using the model developed in Sec. 3.1. In the following study, the heat equation is used to calculate the temperature variation during the different tests. Indeed, the proposed model aims at linking the temperature to the different mechanical parameters.

3.2.1 Nature of the Problem. The energy conservation law (first thermodynamic principle) allows us to write

$$\rho \,.\, \dot{u} = \sigma \,.\, \dot{\varepsilon} + r - \mathrm{div}(\boldsymbol{q}) \quad (24)$$

with u specific internal energy defined by $u=\phi+T$, s; r the internal heat production volume density; $\boldsymbol{q}$ is the heat current vector, where ϕ is defined by Eq. (9) and s by Eq. (13a).

In order to obtain the usual expression of the heat equation, the equation $u=\phi+Ts$ has to be introduced in Eq. (24). Considering

$$\dot{u} = \dot{\phi} + s\dot{T} + T\dot{s} \quad (25)$$

with

$$\dot{\phi} = \frac{\partial\phi}{\partial\varepsilon}\dot{\varepsilon} + \frac{\partial\phi}{\partial T}\dot{T} + \frac{\partial\phi}{\partial z_\sigma}\dot{z}_\sigma + \frac{\partial\phi}{\partial z_T}\dot{z}_T + \frac{\partial\phi}{\partial h}\dot{h} \quad (26)$$

and with

$$\dot{s} = -\left(\frac{\partial^2\phi}{\partial\varepsilon\partial T}\dot{\varepsilon} + \frac{\partial^2\phi}{\partial^2 T}\dot{T} + \frac{\partial^2\phi}{\partial z_\sigma\partial T}\dot{z}_\sigma + \frac{\partial^2\phi}{\partial z_T\partial T}\dot{z}_T + \frac{\partial^2\phi}{\partial h\partial T}\dot{h}\right) \quad (27)$$

we have to calculate

$$\frac{\partial\phi}{\partial\alpha} \text{ and } \frac{\partial^2\phi}{\partial\alpha\partial T} \text{ with } \alpha = (\varepsilon, T, z_\sigma, z_T, h)$$

3.2.2 First Derivative Calculation

$$\frac{\partial\phi}{\partial\varepsilon} = \frac{\sigma}{\rho} \quad (28)$$

$$\frac{\partial\phi}{\partial T} = -s = -C_v\ln\left(\frac{T}{T_0}\right) - s_0^{*(1)} + z\,.\,\Delta s^* - z(1-z)\,.\,s_0 - z_\sigma\,.\,z_T\,.\,s_0^m - s_h^{*(1)} + z\,.\,\Delta s_h^* \quad (29)$$

$$\frac{\partial\phi}{\partial z_\sigma} = z_T\,.\,\phi_{ir}^m - \frac{E\,.\,\gamma}{\rho}(\varepsilon - \gamma\,.\,z - \alpha_0(T-T_0)) - \Delta\Pi_0^f(h,T) - \Pi_0^f(T) + (1-2\,.\,z)\phi_{it} \quad (30)$$

$$\frac{\partial\phi}{\partial z_T} = z_\sigma\,.\,\phi_{ir}^m - \frac{E\,.\,\gamma}{\rho}(\varepsilon - \gamma\,.\,z - \alpha_0(T-T_0)) - \Delta\Pi_0^f(h,T) - \Pi_0^f(T) + (1-2\,.\,z)\phi_{it} \quad (31)$$

$$\frac{\partial\phi}{\partial h} = (\bar{\bar{u}}_1 - T\bar{\bar{s}}_1)\,.\,h - (\overline{u_1} - T\,.\,\overline{s_1}) - \,.\,z\,.\,(\bar{\bar{\phi}}\,.\,h + \bar{\phi}) \quad (32)$$

$\partial\pi/\partial h$ is calculated using Eqs. (15)–(17).

3.2.3 Second Derivatives Calculation

$$\frac{\partial^2\phi}{\partial^2 T} = \frac{-C_v}{T} \quad (33)$$

$$\frac{\partial^2\phi}{\partial\varepsilon\partial T} = -\alpha_0\frac{E}{\rho} \quad (34)$$

$$\frac{\partial^2\phi}{\partial\varepsilon\partial z_\sigma} = -s_0^m z_T + \frac{E\gamma\alpha_0}{\rho} + \Delta s_h^*(h) + \Delta s^* - (1-2z)s_0 \quad (35)$$

$$\frac{\partial^2\phi}{\partial\varepsilon\partial z_T} = -s_0^m z_\sigma + \frac{E\gamma\alpha_0}{\rho} + \Delta s_h^*(h) + \Delta s^* - (1-2z)s_0 \quad (36)$$

$$\frac{\partial^2\phi}{\partial\varepsilon\partial h} = -\bar{\bar{s}}_1 h + \overline{s_1} - z\left(\frac{\partial\bar{\bar{\phi}}}{\partial T}h + \frac{\partial\bar{\phi}}{\partial T}\right) \quad (37)$$

The evolutions of $\bar{\bar{\phi}}$ *and* $\bar{\phi}$ with T are explained in [12,18].

3.2.4 Heat Equation. If we consider that the heat conduction follows an isotropic, linear Fourier law, the heat current vector becomes

$$\boldsymbol{q} = -k\,.\,\boldsymbol{grad}(T) \quad (38)$$

Thus Eq. (24) becomes

$$\rho\dot{u} = \sigma\dot{\varepsilon} + k\Delta T \quad (39)$$

where Δ is the Laplacian operator.

From Eqs. (25) and (39) we can write

$$\rho\dot{u} = \sigma\dot{\varepsilon} + k\Delta T = \rho(\dot{\phi} + s\dot{T} + T\dot{s}) \quad (40)$$

with $\dot{T}$ the particular derivative of T as

$$\dot{T} = \frac{\partial T}{\partial t} + \boldsymbol{v}\,.\,\boldsymbol{grad}(T) \quad (41)$$

where $\boldsymbol{y}$ is the particle speed (negligible for metallic materials load at low rates).

Substituting Eqs. (41) and (28)–(37) in Eq. (40) we obtain the following result, which links the temperature variation to the mechanical parameters:

$$k\Delta T - \rho C_v\frac{\partial T}{\partial t} + \rho\dot{h}Tz\left(\frac{\partial\bar{\bar{\phi}}}{\partial T}h + \frac{\partial\bar{\phi}}{\partial T}\right) = \rho\Bigg(z_T u_0^m - \frac{E\,.\,\gamma}{\rho}(\varepsilon - \gamma\,.\,z + \alpha_0 T_0) - \Delta u_h^* - \Delta u^* + (1-2\,.\,z)u_0\Bigg)\dot{z_\sigma} + \rho\Bigg(z_\sigma u_0^m - \frac{E\,.\,\gamma}{\rho}(\varepsilon - \gamma z + \alpha_0 T_0) - \Delta u_h^* - \Delta u^* + (1-2z)u_0\Bigg)\dot{z_T} - (z(\bar{\bar{\phi}}h + \bar{\phi}))\dot{h}. \quad (42)$$

Numerical results obtained with this equation are presented in Sec. 5.

4 Nonlinear Behavior Modeling

4.1 Equivalent Complex Young's Modulus Notion. The equivalent complex Young's modulus is a powerful tool usually used to describe the elastic behavior and the damping properties of a viscoelastic material under dynamic loading [19,20]. This equivalent modulus can be generalized to quantify, on the first harmonic, the response of a nonlinear hysteretic material.

First of all let us recall that for an isotropic viscoelastic material, the relaxation modulus $E(t)$ is defined by

$$\sigma(t) = \int_{-\infty}^{t} E(t-\tau)\frac{d\varepsilon(\tau)}{d\tau}d\tau \tag{43}$$

where $\sigma(t)$ and $\varepsilon(t)$ are the stress and the strain defined for a uniaxial relaxation test. Furthermore, $E(t)$ is the sum of an asymptotic and a time dependant term

$$E(t) = E_\infty + E^*(t) \tag{44}$$

where $E^*(t) \to 0$ when $t \to \infty$.

Thus, Eq. (43) becomes

$$\sigma(t) = E_\infty \int_{-\infty}^{t} \frac{d\varepsilon(\tau)}{d\tau}d\tau + \int_{-\infty}^{t} E^*(t-\tau)\frac{d\varepsilon(\tau)}{d\tau}d\tau \tag{45}$$

and can be written

$$\sigma(t) = E_\infty \varepsilon(t) + \int_{-\infty}^{t} E^*(t-\tau)\frac{d\varepsilon(\tau)}{d\tau}d\tau \tag{46}$$

By using a Fourier transform on the last equation we obtain

$$\sigma(\omega) = E_\infty \varepsilon(\omega) + i\omega E^*(\omega)\varepsilon(\omega) \tag{47}$$

The complex term $E^*(\omega)$ is defined by

$$E^*(\omega) = E_r^*(\omega) + iE_i^*(\omega) \tag{48}$$

Assuming Eq. (48), Eq. (47) becomes

$$\sigma(\omega) = (E_\infty - \omega E_i^*(\omega) + i\omega E_r^*(\omega))\varepsilon(\omega) \tag{49}$$

which can be written

$$\sigma(\omega) = \bar{E}(\omega)\varepsilon(\omega) \tag{50}$$

where $\bar{E}(\omega)$ is the equivalent complex Young Modulus. It can also be written

$$\bar{E}(\omega) = E(\omega)(1 + i\,\eta_{E(\omega)}) \tag{51}$$

For the SMA, the hypothesis of an hysteretic damping can be stipulated. This assumption entails $E(\omega) = E^0$ and $\eta_{E(\omega)} = \eta^0$, thus

$$\bar{E}(\omega) = E^0(1 + i\eta^0) \tag{52}$$

4.2 Equivalent Complex Youngs Modulus: Application to SMA. If we consider a given vibrating state, the equivalent stiffness and damping of the material can be modeled by the following expression:

$$\bar{E} = E^*(1 + i\eta) \tag{53}$$

In order to reach the harmonical balance on the first harmonic, an energetic equivalence is used. This harmonic balance is a generalization to the Fourier space of the averaging harmonic method developed by Krylov and Bogoliubov [21] and Bogoliubov and Mitropolsky [22].

Defining W_1 and $W_{1/4}$ the strain energy densities, respectively, accumulated during one period of vibration and one quarter of a period,

$$W_1 = \int_0^T \sigma{:}d\varepsilon$$

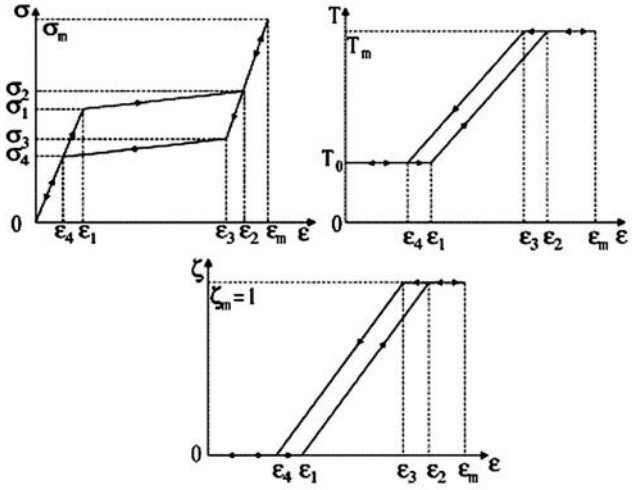

Fig. 13 Simplified nonlinear model of the adiabatic transition

$$W_{1/4} = \int_0^{T/4} \sigma{:}d\varepsilon \tag{54}$$

the harmonic balance leads to

$$W_1 = \pi E^* \eta \varepsilon_m^2$$

$$W_{1/4} = \frac{E^*}{2}\left(1 + \frac{\pi\eta}{2}\right)\varepsilon_m^2 \tag{55}$$

with ε_m the maximum strain during the loading.

It appears that the equivalent complex Young's modulus only depends on the chosen model and should be useful for a finite element simulation. Such approach was used in [23] in order to characterize the pseudoelastic damping behavior of SMA wires. A complete example based on a simplified R_L model is also presented in [1] for the study of a SMA cantilever beam. The simplified R_L is illustrated in Fig. 13. The original contribution of our study consists of studying the influence of cycling on the stiffness variation and damping by computing W_1 and $W_{1/4}$ with the cyclic model presented in Sec. 3. The numerical results of this study are given in the next section.

5 Numerical Results

In this section are presented the results of the numerical simulation on the Ni–Ti used in Sec. 2. The parameters used for these simulations are given in the Appendix.

The first result presented in Fig. 14 is the strain-stress curve obtained with the cyclic model presented in Sec. 3 of this paper. For the 20 cycles presented, the simulation seems to be good from a qualitative point of view. Indeed we can notice a decrease of the outset of the direct phase transformation, an increase of the residual strain with the number of cycle. Besides the experimental tests the most important variation occurs between the first and the second cycle and less significantly between the second and third cycle. At last the appearance of a stabilized cycle can be observed.

For the first and the 20th cycles Figs. 15(a) and 15(b) present the comparison between the experimental and the simulated cycles. For most parameters the results are convincing. For the first cycle the simulation is in very good agreement with the experimental curve. For the 20th cycle the agreement is good for the outset of the direct phase transformation and for the residual strain but the result is less obvious for the outset of the reverse phase transformation. This problem is intrinsic to the proposed model and has to be studied further.

In order to confirm the feeling of these first observations, Figs. 16(a) and 16(b) are proposed. For each cycle between the first and

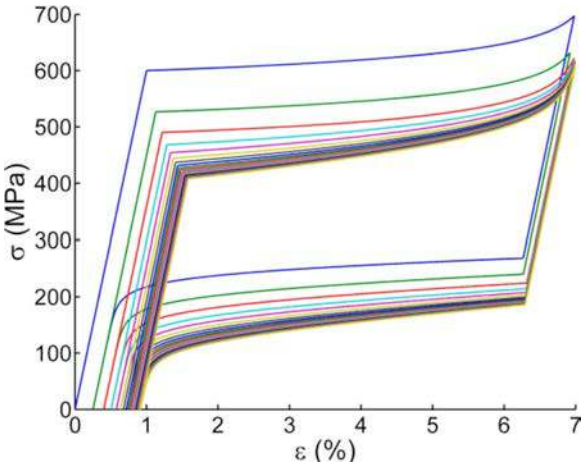

Fig. 14 Ni–Ti quasistatic cyclic test: numerical simulation

the 20th, the outset of the direct phase transformation is well predicted as confirmed by Fig. 16(*a*). In Fig. 16(*b*) we can note the good agreement between the computed and the experimental fraction of residual martensite. The residual fraction of martensite is calculated from the residual strain using Eq. (2).

As a conclusion to the cyclic model, it is important to comment the influence of the cyclic behavior of the Ni–Ti on the nonlinear modeling. In Fig. 17 we can observe on the real part of the equivalent complex Young's modulus that the stiffness decreases with the number of cycles. On the imaginary part the damping seems to increase. This simple observation shows the importance in taking into account the change of the behavior with the cycling to realize a good prediction of the nonlinear behavior thanks to the equivalent complex Young's modulus. At last, predictions of the temperature variations during cyclic tests using the heat equation modeling presented in Sec. 4 are done for the austenitic Cu–Al–

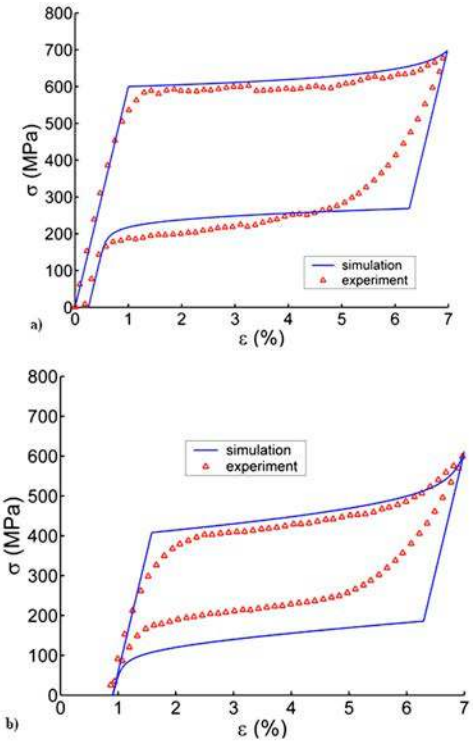

Fig. 15 Ni–Ti quasistatic cyclic test: (*a*) first cycle comparison; (*b*) 20th cycle comparison

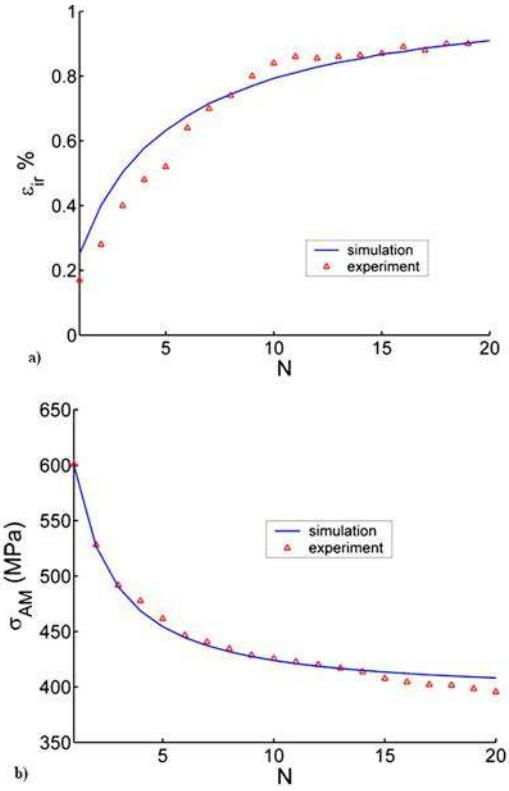

Fig. 16 Ni–Ti quasi-static cyclic test: (*a*) σ_{AM} comparison; (*b*) ε_{ir} comparison

Be. These simulations are realized on 50 cycles. The results for the four strain rates from 10^{-4} to 2×10^{-1} s^{-1} are presented in Figs. 18 and 19. We can observe in these figures that the thermal behavior is well predicted excepted for the strain rate of 2×10^{-1} s^{-1} where a small drift can be noticed. It is important to highlight that the results observed in Sec. 2 for this material allows us to use a weak coupling between mechanical and thermal behaviors.

Conclusions

The cyclic behavior of the three alloys has been experimentally studied. For the Ni–Ti, the strain rate has an important influence on the mechanical behavior, but for the two Cu–Al–Be there are no significant differences on the stabilized cycles with the strain rate. For these two copper alloys, the most important fact to observe is the huge heat dissipation during the cycling.

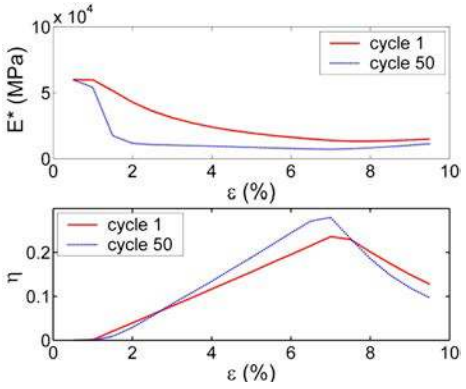

Fig. 17 Equivalent complex Young's modulus: cycle and strain influence for the Ni–Ti

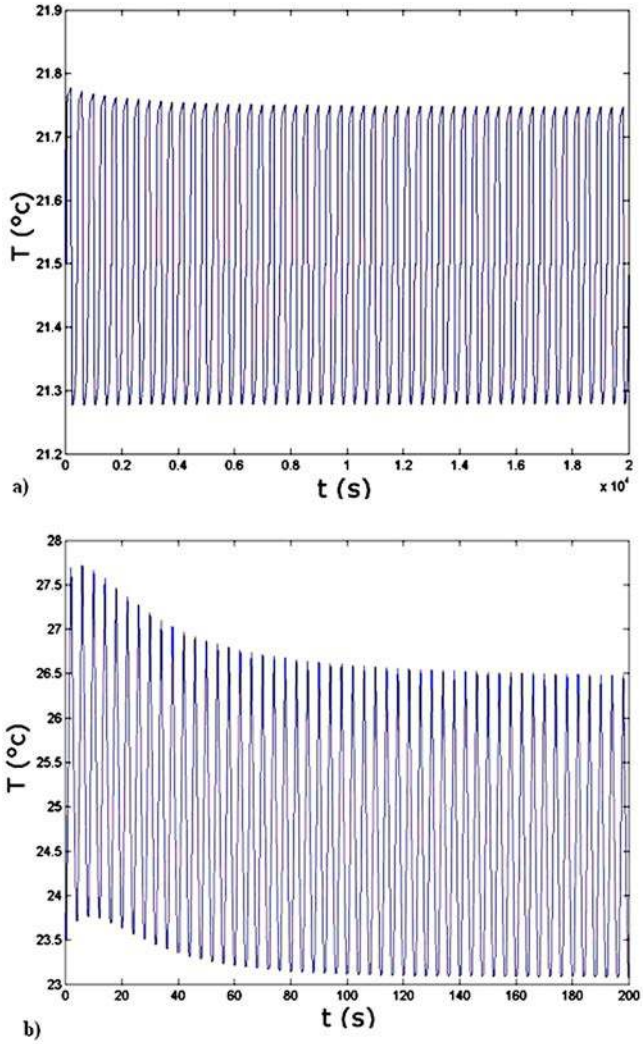

Fig. 18 Cu–Al–Be(1) temperature variation simulation: (*a*) test at 10^{-4} s^{-1}; (*b*) test at 10^{-2} s^{-1}

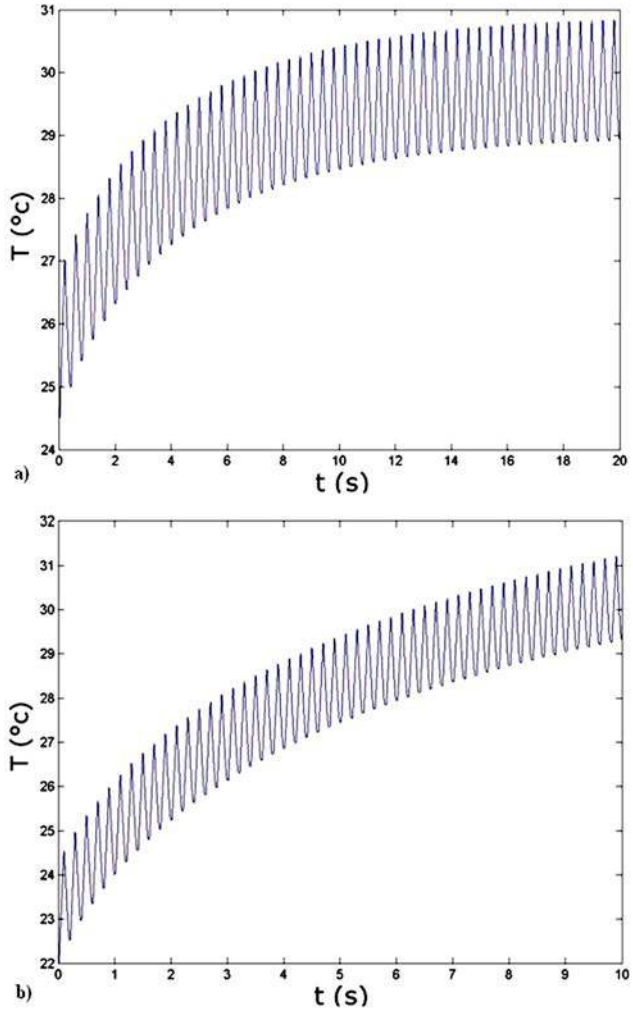

Fig. 19 Cu–Al–Be(1) temperature variation simulation: (*a*) test at 10^{-1} s^{-1}; (*b*) test at 2×10^{-1} s^{-1}

In the second part a model of the cyclic behavior of the SMA based on the notion of residual fraction of martensite was presented. It was built on an R_L model base and a complete study of the heat equation was added in order to be able to predict the temperature variation during the cycling.

In the third part of the paper a simple method was presented in order to model the nonlinear behavior of SMA during dynamical loading. This equivalent complex Young's modulus is a powerful tool to be used with the finite element method for simulations.

At last the results of a few numerical simulations were presented. They show clearly that it is highly important to care about the change of the behavior with the cycling to predict the stiffness and damping variations. Moreover we succeeded in predicting the temperature variations for an austenitic SMA.

In the future, the next step will consist of using the work made on the heat equation in order to compute the temperature during the different tests for martensitic shape memory alloys. Furthermore we want to improve our knowledge of damping on SMA by performing some experiments on Cu–Al–Be wires using a nonlinear identification method based on the wavelet transform.

This study permits us to improve the nonlinear modeling of SMA in order to develop and optimize applications for the control and the damping in civil engineering.

Acknowledgment

Thanks to D. Tirelli from the JRC ISPC laboratory in ISPRA (Italy) for his help and the Ni–Ti samples.

Nomenclature

Physical constants

ρ = material density
E = Young's modulus
α_0 = thermal expansion coefficient

SMA variables

z = total fraction of martensite
z_T = fraction of self-accommodated martensite
z_σ = fraction of oriented martensite
h = fraction of residual martensite
γ = maximum strain associated with a complete phase transformation
M_s^0 = martensitic transformation start temperature
M_f^0 = martensitic transformation end temperature
A_s^0 = austenitic transformation start temperature
A_f^0 = austenitic transformation end temperature
σ_{AM} = outset stress of the direct phase transformation $A \rightarrow M$

σ_{MA} = outset stress of the reverse phase transformation $M \rightarrow A$
α = 1 for the austenite
α = 2 for the oriented martensite, 3 for the self-accommodated martensite

Mechanical variables

ε = total strain
ε_{ir} = residual strain at a free stress state
ε_T = total thermal strain
$\varepsilon^{(\alpha)}$ = α phase strain
$\varepsilon_T^{(\alpha)}$ = α phase thermal strain
σ = strain

Thermodynamical variables and functions

T = system temperature
T_0 = reference temperature
C_v = specific heat
$\underline{u_0}$ = system configuration internal energy
$\underline{s_0}$ = system configuration entropy
ϕ_{it} = system configuration free specific energy
$\phi_{(\alpha)}$ = α phase free specific energy
ϕ = biphased system free specific energy
$u_0^{*(\alpha)}$ = α phase internal energy at reference state
$s_o^{*(\alpha)}$ = α phase entropy at reference state
Π_0^f = temperature induce phase transformation at free stress state driving force
Π_α^f = phase transformation driving force (associated with z_α, α=T, σ)
Π^h = phase transformation driving force (associated with h)
$\psi^{(\alpha)}$ = α phase transformation yield function
$k^{(\alpha)}$ = α phase transformation kinetic
s = system specific entropy
u = system free energy
q = system specific heat transfer
$\Delta\Pi_0^f$ = thermodynamic force associated with h
$\bar{\bar{\phi}}, \bar{\phi}$ = T functions defining $\Delta\Pi_0^f$
m_0, p = constants associated with h kinetics
h_∞ = h saturation value

Appendix: Simulations Main Parameters

Ni–Ti

ρ = 6500 kg m^{-3}
E = 60,000 MPa
α_0 = 11e^{-6} K^{-1}
γ = 6%
M_s^0 = 213 K
A_s^0 = 248 K
$\underline{u_0}$ = 1997 J Kg^{-1}
s_0 = 3.13 J kg^{-1} K^{-1}
$\Delta\bar{u}$ = 15,898 J kg^{-1}
$\Delta\bar{s}$ = 68 J kg^{-1} K^{-1}
$\bar{\bar{\phi}}$ = 70,000 J kg^{-1}
h_∞ = 0.2
m_0 = 2.1
p = 1

Cu–Al–Be(1)

ρ = 7500 kg m^{-3}
E = 75,000 MPa
α_0 = 17e^{-6} K^{-1}
γ = 6%
M_s^0 = 213 K
A_s^0 = 253 K
C_v = 794 J kg^{-1} K^{-1} @25°C
$\underline{u_0}$ = 472 J kg^{-1}
s_0 = 0 J kg^{-1} K^{-1}
$\Delta\bar{u}$ = 5600 J kg^{-1}
$\Delta\bar{s}$ = 24 J kg^{-1} K^{-1}
$\bar{\bar{\phi}}$ = 100,000 J kg^{-1}
h_∞ = 0.3
m_0 = 10
$\underline{p}$ = 1.1
u_1 = 9.7e^4 J kg^{-1}
$\bar{\bar{u}}_1$ = 1.8e^6 J kg^{-1}

References

[1] Saadat, S., Saliche, J., Noori, M., Hou, Z., and Davoodi, H., 1999, "Promises for Structural Vibration Control (SVC) Using Shape Memory Alloys," Int. J. Mech. Sci., **43**, pp. 2631–2656.

[2] Dolce, M., and Cardone, D., 2001, "Mechanical Behaviour of Shape Memory Alloys for Seismic Applications. 1. Martensite and Austenite Ni–Ti Bars Subjected to Torsion," Int. J. Mech. Sci., **43**, pp. 2631–2656.

[3] Dolce, M., and Cardone, D., 2001, "Mechanical Behaviour of Shape Memory Alloys for Seismic Applications. 2. Austenite Ni–Ti Wires Subjected to Tension," Int. J. Mech. Sci., **43**, pp. 2657–2677.

[4] Collet, M., Foltête, E., and Lexcellent, C., 2001, "Analysis of the Behavior of a Shape Memory Alloy Under Dynamical Loading," Eur. J. Mech. A/Solids, **20**, pp. 615–630.

[5] Raniecki, B., and Lexcellent, C., 1994, "R_L Models of Pseudoelasticity and Their Specifications for Shape Memory Solids," Eur. J. Mech. A/Solids, **13**, pp. 21–50.

[6] Tobushi, H., Shimeno, Y., Hachisuka, T., and Tanaka, K., 1998, "Influence of Strain Rate on Superelastic Properties of TiNi Shape Memory Alloy," Mech. Mater., **30**, pp. 141–150.

[7] Strnadel, B., Ohashi, S., Otsuka, H., Miyazaki, S., and Ishihara, T., 1995, "Effect of Mechanical Cycling on the Pseudoelasticity Characteristics of Ti–Ni and Ti–Ni–Cu Alloys," Mater. Sci. Eng., A, **203**, pp. 187–196.

[8] Liu, Y., Xie, Z., and VanHumbeeck, J., 1999, "Cyclic Deformation of Ni–Ti Shape Memory Alloys," Mater. Sci. Eng., A, **273**, pp. 273–375; 1999, Mater. Sci. Eng., A, **273**, pp. 673–678.

[9] Piedboeuf, M. C., and Gauvin, R., 1998, "Damping Behaviour of Shape Memory Alloys: Strain Amplitude, Frequency and Temperature Effects," J. Sound Vib., **214**(5), pp. 885–901.

[10] Cedip Infrared web site, http://www.cedip-infrared.com

[11] Ortin, J., 1992, "Preisach Modeling of Hysteresis for a Pseudoelastic Cu–Zn–Al Single Crystal," J. Appl. Phys., **71–3**, pp. 1454–1461.

[12] Lexcellent, C., and Bourbon, G., 1996, "Thermodynamical Model of Cyclic Behavior of Ti–Ni and Cu–Zn–Al Shape Memory Alloys Under Isothermal Undulated Tensile Tests," Mech. Mater., **24**, pp. 59–73.

[13] Auricchio, F., Marfia, S., and Sacco, E., 2003, "Modelling of SMA Materials: Training and Two Way Memory Effects," Comput. Struct., **81**, pp. 2301–2317.

[14] Abeyaratne, R., and Kim, S.-J., 1997, "Cyclic Effects in Shape Memory Alloys: A One-Dimensional Continuum Model," Int. J. Solids Struct., **34–25**, pp. 3273–3289.

[15] Lim, T. J., and McDowell, D. L., 2002, "Cyclic Thermomechanical Behavior of a Polycrystalline Pseudoelastic Shape Memory Alloy," J. Mech. Phys. Solids, **50**, pp. 651–676.

[16] Leclerq, S., and Lexcellent, C., 1996, "A General Macroscopic Description of the Thermomechanical Behavior of Shape Memory Alloys," J. Mech. Phys. Solids, **44**, pp. 953–980.

[17] Miyazaki, S., 1990, "Thermal and Stress Cycling Effect and Fatigue Properties of Ni–Ti Alloys," *Engineering Aspect of Shape Memory Alloy*, T. W. Duerig et al., ed., Butterworth-Heinemann, London, pp. 394–413.

[18] Bourbon, G., 1994, "Contribution à l'Étude Isotherme et Anisotherme du Comportement Cyclique des Alliages à Mémoire de Forme," Thése No. 410, Université de Franche Comté, France.

[19] Caracciolo, R., Gasparetto, A., and Giovagnoni, M., 2004, "An Experimental Technique for Complete Dynamic Characterization of a Viscoelastic Material," J. Sound Vib., **272**, pp. 1013–1032.

[20] Pintelon, R., Guillaume, P., Vanlanduit, S., De Belder, K., and Rolain, Y., 2004, "Identification of Young's Modulus from Broadhand Modal Analysis Experiment," Mech. Syst. Signal Process., **18**, pp. 699–726.

[21] Krylov, N., and Bogoliubov, N., 1943, *Introduction to Nonlinear Mechanics*, Princeton University Press, Princeton, New Jersey.

[22] Bogoliubov, N., and Mitropolsky, J., 1963, *Asymptotical Methods in the Theory of Nonlinear Oscillations*, State Press for Physics and Mathematical Literature, Moscow.

[23] Gandhi, F., and Wolons, D., 1999, "Characterisation of the Pseudoelastic Damping Behavior of Shape Memory Alloy Wires Using Complex Modulus," Smart Mater. Struct., **8**, pp. 49–56.